Effects of deposition methods and processing techniques on band gap, interband electronic transitions, and optical absorption in perovskite $CH_3NH_3PbI_3$ films

Wenwu Li (李文武),[1,a)] Tingting Sha (沙婷婷),[1] Yan Wang (王琰),[2] Wenlei Yu (余温雷),[3] Kai Jiang (姜凯),[1] Hang Zhou (周航),[2,a)] Chuan Liu (刘川),[4] Zhigao Hu (胡志高),[1,a)] and Junhao Chu (褚君浩)[1]

[1]*Key Laboratory of Polar Materials and Devices (Ministry of Education), Technical Center for Multifunctional Magneto-Optical Spectroscopy (Shanghai), East China Normal University, Shanghai 200241, China*
[2]*School of Electronic and Computer Engineering, Peking University Shenzhen Graduate School, Peking University, Shenzhen 518055, China*
[3]*Department of Biomedical Engineering, Wenzhou Medical University, Zhejiang 325035, China*
[4]*State Key Laboratory of Optoelectronic Materials and Technologies, Guangdong Province Key Laboratory of Display Material and Technology, School of Electronics and Information Technology, Sun Yat-Sen University, Guangzhou 510275, China*

(Received 1 April 2017; accepted 23 June 2017; published online 6 July 2017)

Despite intensive studies on the improvements of conversion efficiencies in solar cells, many questions regarding the effects of deposition techniques on optical properties and electronic band structures of $CH_3NH_3PbI_3$ ($MAPbI_3$) remain unresolved. Here, perovskite $MAPbI_3$ films were prepared using different deposition methods and processing techniques. The effects of deposition and processing parameters on dielectric functions and optical absorption were investigated by fitting the reflectance spectra in the photon energy range of 0.5–5.16 eV. It is found that the bandgap (E_g) of the films deposited by two-step spinning (1.591 eV) is larger than that prepared by evaporations (1.514 eV), due to different Pb-I orbital hybridization and spin-orbit coupling. Moreover, the E_g value of the films increases from 1.543 eV to 1.591 eV after toluene solution dripping. Five interband electronic transitions (E_{p1}, E_{p2}, E_{p3}, E_{p4}, and E_{p5}) are observed, and the origins of E_{p2}, E_{p3}, and E_{p4} are assigned to the direct transitions between the highest valence band and the lowest lying conduction band at the R, M, and X symmetry points. Further, the transition energies of the films deposited by evaporation are less than those prepared by two-step spinning. The present results shed light on preparing more reliable and reproducible high performance $MAPbI_3$-based solar cells. *Published by AIP Publishing.* [http://dx.doi.org/10.1063/1.4991864]

Perovskite solar cells (PSCs) have attracted considerable interest because of their potential for low-cost, large-scale, and high efficiency solar energy production. After only 5 years of development, lead halide perovskite solar cells have reached certified power conversion efficiencies over 22.1%, which is an unprecedented achievement compared to the counterparts using conventional materials.[1–3] More importantly, there is no sign indicating that the energy conversion efficiency of PSCs has reached a bottleneck. As light-harvesting materials, organic-inorganic hybrid perovskites such as $CH_3NH_3PbX_3$ ($MAPbX_3$) (X = Cl, Br, and I) have been widely studied, with promising properties such as a suitable optical bandgap (E_g) of 1.57 eV,[4] large absorption coefficient ($10^4\,cm^{-1}$),[5] high carrier mobility, and long charge carrier diffusion length (1 μm).[6,7] These excellent optical and electrical properties make $CH_3NH_3PbI_3$ ($MAPbI_3$) an efficient absorber material for applications in perovskite solar cells.

Developing a deeper understanding of the optical properties is important both practically and theoretically for solar cells. A suitable bandgap and a high absorption coefficient for absorber materials play an important role in determining the energy conversion efficiency of photovoltaic devices. Bandgap tuning is required to extend the absorption to longer wavelengths without sacrificing the absorption coefficient. Many efforts have been made to optimize the bandgap and absorption of the $MAPbI_3$ layer.[5,8] Modification of the bond distance and/or angle of X-Pb-X in $MAPbI_3$ is one of the strategies to affect bandgap energy. A theoretical study suggests that the bandgap can also be adjusted by the *p* orbital of I and *p* orbital of Pb.[9]

Low-cost and facile deposition techniques are desired to fabricate stable and high quality $MAPbI_3$ films. Compared to one-step methods, two-step spin-coating processing[10,11] and thermal evaporation methods,[12] which are very important techniques for absorption layer fabrications, exhibit better photovoltaic performance owing to better morphology and interfaces.[13] It should be noted that the phase transition, microstructure, defect states, and optical properties of $MAPbI_3$ films are strongly affected by temperatures and deposition methods. Jiang *et al.* reported the temperature dependent optical properties of $MAPbI_3$ films from 77 K to room temperature.[14] Furthermore, the bandgap, optical constants, and optical absorption can also be affected by processing techniques such as toluene dripping treatment. However, a fundamental experimental understanding for the

[a)]Authors to whom correspondence should be addressed: wwli@ee.ecnu.edu.cn; zhouh81@pkusz.edu.cn; and zghu@ee.ecnu.edu.cn

electronic band structure, bandgap energy, and optical absorption in addition to the deposition methods is still lacking.

In this work, the perovskite $CH_3NH_3PbI_3$ films were fabricated on Al_2O_3/Si substrates by different deposition methods and processing techniques. The effects of the fabrication techniques on the electronic transitions and the physical mechanism have been discussed in detail.

The $MAPbI_3$ films were deposited with four different methods on the Al_2O_3/Si substrate, as shown in Fig. 1. An Al_2O_3 thin film with a thickness of 3 nm was applied as an inert layer on a silicon substrate to improve the film density, uniformity, and crystal quality of the perovskite films. For sample A, the main precursor PbI_2 was first fabricated into a uniform and compact film by vapor deposition. Afterwards, the PbI_2 film was immediately immersed in a bath of CH_3NH_3I (MAI) solvent (10 mg/ml) for 10 min. For sample C, the precursor PbI_2 was prepared in dimethylformamide (DMF) solution followed by spin-coating at a speed of 3000 rpm for 40 s. Then, the MAI solution (10 mg/ml) was dipped onto the PbI_2 film by spin-coating (2000 rpm/60 s). Therefore, the MAI solution intercalates into the PbI_2 precursor film to form $MAPbI_3$ perovskite. For sample B and sample D, toluene dripping treatment was finally applied to improve the uniformity in addition to the fabrication process of sample A and sample C. All the samples were cleaned by isopropyl alcohol (IPA) at a speed of 2000 rpm for 20 s and then annealed at 100 °C for 30 min. The reflectance spectra were measured at room temperature with a double beam ultraviolet-infrared spectrophotometer (Perkin Elmer Lambda 950) in the photon energy range of 0.5 to 5.16 eV (240–2500 nm) with a spectral resolution of 2 nm.

Comprehensive studies of optoelectronic properties of $MAPbI_3$ films are needed for establishing robust optical models to improve the design of solar cells. The reflectance technique is a nondestructive and powerful tool for the optical characterization of semiconductor film materials, which can directly provide electronic band energy and dielectric constants. Moreover, spectral reflectance has been applied to obtain optical functions of semiconductor and dielectric materials.[15,16] The experimental reflectance spectra of the $MAPbI_3$ films with different deposition methods and processing techniques are plotted in Fig. 2 by dotted lines. The

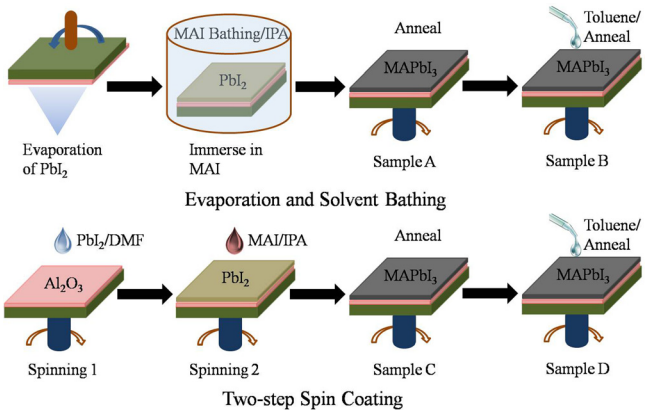

FIG. 1. Schematic illustration of the different deposition methods and processing techniques to obtain $MAPbI_3$ films.

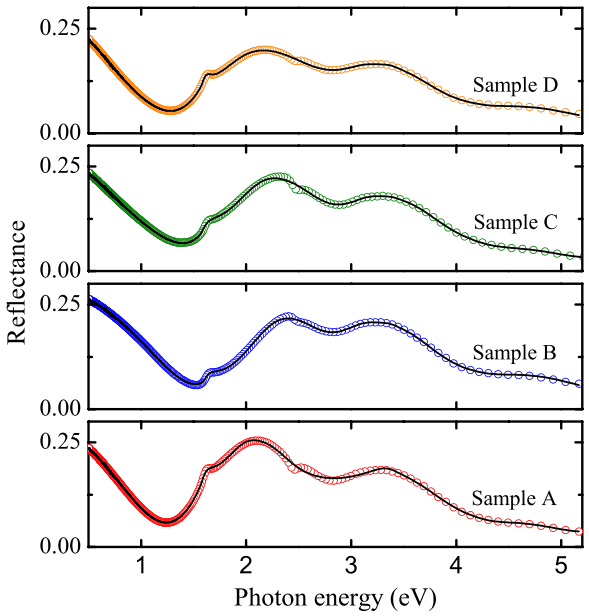

FIG. 2. The experimental (dotted lines) and model-fit (solid lines) reflectance spectra of $MAPbI_3$ films with different deposition methods and processing techniques in the photon energy range of 0.5 to 5.16 eV.

well-known absorption edge at about 1.5 eV can be observed from the spectra, which is similar to the results reported by Löper *et al.*[6] One can find that the reflection characteristics in sub-band regions and at fundamental absorption edge depend strongly on the deposition methods. It suggests that the electronic transition and optical bandgap are different among samples, which indicates different electronic band structures and crystalline quality. Note that small features at about 2.45 eV (about 505 nm) can be observed from the spectra, which can be attributed to the small amount of the PbI_2 component remaining in $MAPbI_3$ films.[17]

The inverse synthesis method is based on a phenomenological model fitted to the experimental results. A three-phase layered structure (air/film/substrate) was constructed for each sample to determine the optical properties of the $MAPbI_3$ films. The optical constants of the substrate (Al_2O_3/Si), which is used for determining the dielectric functions of $MAPbI_3$ films, can be obtained from the commercial database. The optical transition numbers and position energies of $MAPbI_3$ films have been reported by many research groups. More than eight Tauc-Lorentz (TL) oscillators have been applied to extract the transition energies in a wide photon energy range.[18] However, only five transitions located within the measured photon range of this work. Therefore, the dielectric functions of the $MAPbI_3$ films were extracted by fitting the reflectance spectra with five TL oscillators[19,20]

$$\varepsilon_1(E) = \varepsilon_\infty + \frac{2}{\pi} P \int_0^\infty \frac{\xi \varepsilon_2(E)}{\xi^2 - E^2} d\xi;$$
$$\varepsilon_2(E) = \sum_{i=1}^{5} \frac{A_i E_{pi} \Gamma_i (E - E_{ti})^2}{\left(E^2 - E_{pi}^2\right)^2 + \Gamma_i^2 E^2} \frac{1}{E}, \quad (1)$$

where ε_∞ is the high-frequency dielectric constant, P is the Cauchy principal part of the integral, E is the incident photon energy, and A_i, E_{pi}, Γ_i, and E_{ti} are the amplitude, transition

TABLE I. The electronic transition energy for $MAPbI_3$ films with different deposition methods are determined from the simulation of the reflectance spectra using the five Tauc-Lorentz oscillator model.

Samples	Thickness (nm)	ε_∞	E_{p1} (eV)	E_{p2} (eV)	E_{p3} (eV)	E_{p4} (eV)	E_{p5} (eV)
A	104 ± 1	3.51 ± 0.02	1.14 ± 0.21	1.58 ± 0.03	2.22 ± 0.02	2.79 ± 0.13	4.68 ± 0.09
B	98 ± 1	3.44 ± 0.02	1.20 ± 0.02	1.60 ± 0.01	2.57 ± 0.01	3.26 ± 0.03	4.76 ± 0.05
C	105 ± 1	3.22 ± 0.01	1.34 ± 0.03	1.57 ± 0.03	2.46 ± 0.02	3.27 ± 0.05	4.69 ± 0.05
D	111 ± 1	2.91 ± 0.01	1.40 ± 0.03	1.61 ± 0.01	2.36 ± 0.01	3.24 ± 0.05	4.72 ± 0.04

position energy, broadening term, and Tauc gap energy of the *i*th oscillator, respectively. The thickness of the film is one of the fitting parameters, which can be obtained by fitting the reflectance spectra. The TL model, which follows by the Kramers-Krönig transformation in the entirely measured photon energy region, is applied in many semiconductor materials. The best-fit reflectance data with the TL model are plotted in Fig. 2 by solid lines, which illustrates that this model reproduces the experimental spectra well.

The fitted parameter values and film thickness are summarized in Table I. The thickness of $MAPbI_3$ films was estimated in the range of 98 nm to 111 nm. As can be seen in Table I, the ε_∞ value of the film decreases after processing with toluene solution. Considering that the high frequency dielectric constant and refractive index (n) are related by $\varepsilon_\infty \propto n$, it indicates that the refractive index decreases with toluene treatments. The energy positions of five transitions (from E_{p1} to E_{p5}) are different with samples, which suggests that the deposition methods can strongly affect the band structure and electronic transitions. The dielectric functions not only provide basic optical properties but also are important for device design. The evaluated dielectric functions of $MAPbI_3$ films are shown in Figs. 3(a) and 3(b). The evolutions of dielectric functions and fundamental peaks show different behaviors using deposition methods and processing techniques. The number of optical electronic transition is related to the physical properties of the $MAPbI_3$ films. Based on the experimental observations[14] and theoretical calculations,[21] five electronic transitions at the photon energy from ultraviolet to near-infrared can be assigned. The five features can also be clearly identified from the ε_2 curves [see Fig. 3(b)] and the physical origins of the electronic transitions will be discussed later.

For absorber layer materials, the absorption coefficient $\alpha = 4\pi k/\lambda$ is one of the most important parameters for their photovoltaic applications. Figure 4 shows the absorption coefficient α of the perovskite $MAPbI_3$ films from different deposition methods. In the region of 0.5–1.5 eV, an absorption edge appears for all films due to the band to band transition. The sharp absorption onset near the bandgap energy indicates that there is low Urbach energy, which is expected to reduce the open-circuit voltage loss. The sharp absorption feature may also result from a discrete excitonic state enhancing absorption in this region. Light penetration through the $MAPbI_3$ layer and the resulting carrier generation depend entirely on α of the $MAPbI_3$ materials. At the photon energy of 2.0 eV, the α values change from 7.9×10^4 to 8.4×10^4 cm^{-1}, which are much higher than those observed from the films fabricated by the two-step evaporation technique (3.8×10^4 cm^{-1}).[22] It indicates that these films contain less voids and the film structures are highly uniform. The variation of optical absorption in the visible region (1.5 eV $\leq E \leq$ 2.5 eV) can be characterized by a featureless nonexcitonic interband transition in the Brillouin zone and the free electrons and holes are generated directly by optical absorption at $E \geq E_g$. Moreover, the optical absorption of $MAPbI_3$ films can be expressed by traditional semiconductor-type optical transitions.[22]

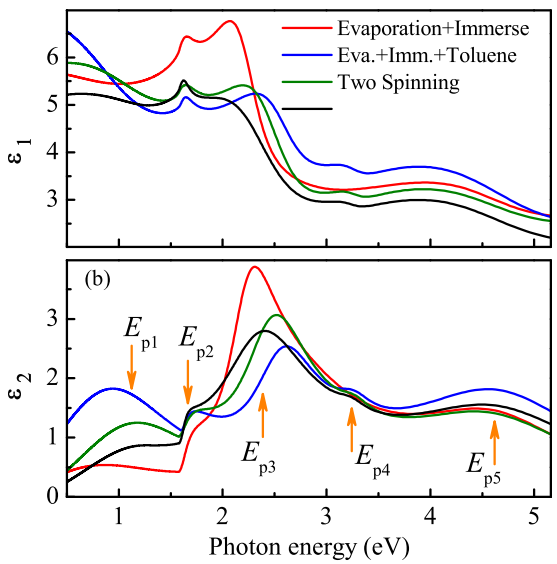

FIG. 3. Fabrication technique dependence of the dielectric functions: (a) real part ε_1 and (b) imaginary part ε_2 of $MAPbI_3$ films in the photon energy range of 0.5–5.16 eV. The arrows indicate the energy positions of the electronic transitions.

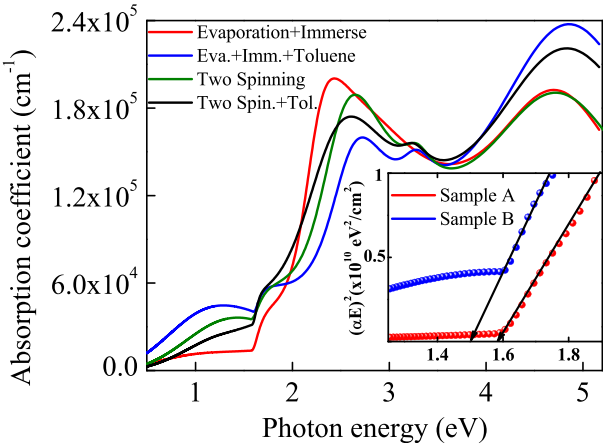

FIG. 4. The absorption coefficient α of different perovskite $MAPbI_3$ samples. The inset shows the variations of $(\alpha E)^2$ with the photon energy E of sample A (red dots) and sample B (blue dots), which are used to determine the bandgap energy E_g.

The bandgap energy of the $MAPbI_3$ films can be calculated by considering direct transitions between the valence band (VB) and the conduction band (CB) when the photon excitation is applied. The power law behavior of Tauc $(\alpha E)^2 \propto (E - E_g)$ was applied for allowed direct transition; here, E is the incident photon energy and E_g is the bandgap energy. The straight line between $(\alpha E)^2$ and E will provide the E_g value, which is extrapolated by the linear portion of the plot to $(\alpha E)^2 = 0$, as seen in the inset of Fig. 4. The extrapolated E_g energies for Sample A, Sample B, Sample C, and Sample D are 1.501, 1.514, 1.543, and 1.591 eV, respectively. The values, which are lower than that deposited by the gas-assisted technique ($E_g = 1.61$ eV),[14] are close to the optimal bandgap ($E_g = 1.5$ eV) for photovoltaic applications. It can be found that the E_g of the films deposited by evaporations is smaller than that prepared by two-step spinning. Moreover, the E_g of the films increases after toluene solution dripping. Theoretical calculations have suggested that the electronic structure of $MAPbI_3$ is related to the p orbital of I and the p orbital of Pb. Further, the bandgap of $MAPbI_3$ films is formed between the unoccupied Pb p orbital and the occupied I p orbital.[23] Finally, according to the Fermi Golden rule, a smaller bandgap will result in a higher probability of optical transitions.

Determination of the optical transition is vital for a clear understanding of the operational principles of $MAPbI_3$ photovoltaic devices. Before assigning the origins of optical transition, the electronic band structures of $MAPbI_3$ materials need to be discussed. The valence band maximum (VBM) and conduction band minimum (CBM) lie at the same point in reciprocal space (k-space). The CBM originates primarily from the Pb 6p states hybridized with a small amount of the I 5s states σ-antibonding and Pb 6p states hybridized with I 5p states π-antibonding orbitals. The VBM can be mainly constructed from three parts: (i) a Pb 6s-I 5p σ-antibonding orbital in the top of the states, (ii) I 5p orbitals in the middle energy region, and (iii) Pb 6p-I 5s σ-bonding and Pb 6p-I 5p π-bonding orbitals in the bottom of the state.[24,25] Table I summarizes all of the optical transition energies extracted from reflectance spectra using the Tauc-Lorentz model. For the present $MAPbI_3$ films, five electronic transition energies can be obtained from the model fitting results and are labeled with E_{p1}, E_{p2}, E_{p3}, E_{p4}, and E_{p5}, respectively. The energy values observed in the present study are similar to those found by experiments and theoretical calculations in other $MAPbI_3$ materials.[14,22,26] The transition energies of the films deposited by evaporations are smaller than those prepared by two-step spinning. In addition, the transition energies increase after toluene solution dripping. The addition of toluene solution into $MAPbI_3$ films might control the crystal growth and reduce the defects in the perovskite layers, which are effective for obtaining highly uniform perovskite films.

Although the tetragonal phase is the most stable phase at room temperature, the cubic phase can also be observed from other perovskite $MAPbI_3$ films.[18,26,27] To discuss the optical transition within the band structure of the perovskite, we assume that the perovskite films are simple pseudocubic structures at room temperature. This is an acceptable approximation of the band structure since the transition from the tetragonal to the pseudo-cubic phase is a second order transition (unlike the 1st order orthorhombic to tetragonal transition). It will result in only a 2% change in the lattice parameters relative to the tetragonal structure at room temperature.[26,28] Moreover, the dielectric functions with the photon energy are similar to the optical response behaviors from experimental measurements and theoretical predictions of reported pseudocubic $MAPbI_3$ films.[18,22] Therefore, this assumption is acceptable and critical to reproduce the optical transitions in the $MAPbI_3$ perovskite. Thus, we used R, M, and X symmetry points in the Brillouin zone of the pseudocubic phase for optical transition discussion.

Note that the optical transition energies, which can also be observed for the ε_2 spectra, reproduce well with the $MAPbI_3$ films with a pseudocubic structure. The majority characteristics of the $MAPbI_3$ films correspond to the different direct electronic transitions between the highest VB and lowest lying CB at the R, M, and X symmetry points. The higher-energy transitions might originate from the highest VB to a second-lowest CB and various second-highest VBs to the lowest lying CB. The lowest energy transition E_{p1} occurs between the doubly degenerate VB and the lower split-off CB. The giant spin-orbit splitting of the Pb-derived CB and I-derived VB states, which are initially split by the crystal fields due to atomic relaxations, can also affect the transition. The E_{p2} feature at about 1.6 eV can be assigned to direct transition from the highest VB to the lowest CB at the R symmetry point in the first Brillouin zone. In addition, the interaction with $CH_3NH_3^+$ can also affect the amplitude of the transition. Similarly, the E_{p3} transition at about 2.5 eV can be assigned to the direct optical transitions from the highest VB to the lowest CB at the M point in the pseudocubic Brillouin zone. The transitions between the highest VB and the second-lowest CB at the R point might also have a minor contribution. The fourth transition is related to the excitation of electrons from the highest VB to the lowest CB at the X point.[26,29] For the highest energy transition E_{p5}, the similar energy positions have been observed from the $MAPbI_3$ films prepared using laser evaporation processing (4.726 eV)[22] and one-step spin coating (4.60 eV).[30] Many research groups try to interpret the origins from theoretical and experimental perspectives, but the physical origins of this transition remain unclear. The E_{p5} can be temporarily attributed to the transition from the highest VB to the second/third lowest CB. More extensive theoretical studies, such as density-functional theory calculations, are desirable to determine the physical origins of optical transitions of the $MAPbI_3$ films. The different deposition methods and processing techniques will result in the changes of crystalline quality, microstructure, density, and morphology in $MAPbI_3$ films, which further affect the optoelectronic properties such as electronic transitions, dielectric functions, and optical absorption.

As shown above, the bandgap, electronic transitions, and optical absorption of the $MAPbI_3$ films can be adjusted by different deposition techniques and toluene processing. Although these strategies represent the mainstream low-cost and facile methods for perovskite film productions, the film qualities such as uniformity, grain size, and compactness are different. For the evaporation methods, the bottom of the film usually exhibits small amounts of PbI_2 residue. The

$MAPbI_3$ films with PbI_2 residue can change the optical properties and usually lead to the low performance in solar cells especially in photocurrent density.[23] For the spin-coating methods, the reaction rate between PbI_2 and MAI solutions is high. Furthermore, the toluene dripping will achieve a compact, smooth, and uniform perovskite film on the substrate. Therefore, larger grain sizes, which results in pinhole-free perovskite films, can be obtained for better charge-transport properties. The grain boundaries of the film can be reduced at the same time. Taking into account the differences of these deposition methods, the evolutions of electronic band structures and optical properties in the $MAPbI_3$ films might be ascribed to the contributions from different uniformities, compactness, defect states, grain sizes, and grain boundaries.

In summary, the dielectric functions, optical bandgap, and optical absorption of the perovskite $MAPbI_3$ films have been investigated using reflectance spectra in the photon energy range of 0.5 eV to 5.16 eV. It can be found that the dielectric functions and absorption coefficient strongly depend on the deposition and processing techniques. The bandgap can be adjusted from 1.591 eV to 1.501 eV using different deposition methods and processing techniques due to different Pb-I orbital hybridization and spin-orbit coupling. Five interband electronic transitions can be observed at about 1.27 eV, 1.59 eV, 2.40 eV, 3.14 eV, and 4.71 eV, which can be attributed to the direct semiconductor-type transitions at the different points in the pseudocubic Brillouin zone, respectively. The transition energies of the $MAPbI_3$ films deposited by evaporations are less than those prepared by two-step spinning. In addition, the transition energies increase after toluene solution dripping.

This work was financially supported by the Major State Basic Research Development Program of China (Grant No. 2013CB922300), the Natural Science Foundation of China (Grant Nos. 61674057, 61504043, 11374097, 61376129, and 61227902), Projects of Science and Technology Commission of Shanghai Municipality (Grant Nos. 14XD1401500 and 15JC1402100), the Program for Professor of Special Appointment (Eastern Scholar) at Shanghai Institutions of Higher Learning, Shenzhen Science and Technology Innovation Fund (JCYJ20150629144006876), the Natural Science Foundation of Zhejiang province (Grant No. LQ16F050005), Wenzhou Science and Technology Bureau (Grant No. G20150025), and the Scientific Research Fund of Zhejiang Provincial Education Department (Grant No. Y201534166).

[1]J. Burschka, N. Pellet, S. J. Moon, R. Humphry-Baker, P. Gao, M. K. Nazeeruddin, and M. Grätzel, Nature **499**, 316 (2013).
[2]J. M. Ball, S. D. Stranks, M. T. Hörantner, S. Hüttner, W. Zhang, E. J. W. Crossland, I. Ramirez, M. Riede, M. B. Johnston, R. H. Friend, and H. J. Snaith, Energy Environ. Sci. **8**, 602 (2015).
[3]S. Wang, Y. Jiang, E. J. Juarez-Perez, L. K. Ono, and Y. Qi, Nat. Energy **2**, 16195 (2016).
[4]H.-S. Kim, C.-R. Lee, J.-H. Im, K.-B. Lee, T. Moehl, A. Marchioro, S.-J. Moon, R. Humphry-Baker, J.-H. Yum, J. E. Moser, M. Grätzel, and N.-G. Park, Sci. Rep. **2**, 591 (2012).
[5]N. G. Park, Mater. Today **18**, 65 (2015).
[6]P. Löper, M. Stuckelberger, B. Niesen, J. Werner, M. Filipič, S.-J. Moon, J.-H. Yum, M. Topic, S. D. Wolf, and C. Ballif, J. Phys. Chem. Lett. **6**, 66 (2015).
[7]G. C. Xing, N. Mathews, S. Y. Sun, S. S. Lim, Y. M. Lam, M. Graetzel, S. Mhaisalkar, and T. C. Sum, Science **342**, 344 (2013).
[8]X. Zhu, R. A. Marcus, and M. E. Michel-Beyerle, J. Phys. Chem. Lett. **5**, 3061 (2014).
[9]E. Mosconi, A. Amat, M. K. Nazeeruddin, M. Grätzel, and F. De Angelis, J. Phys. Chem. C **117**, 13902 (2013).
[10]N. J. Jeon, J. H. Noh, Y. C. Kim, W. S. Yang, S. C. Ryu, and S. Seok, Nat. Mater. **13**, 897 (2014).
[11]J. K. Im, H. S. Kim, and N. G. Park, APL Mater. **2**, 081510 (2014).
[12]M. Z. Liu, M. B. Johnston, and H. J. Snaith, Nature **501**, 395 (2013).
[13]H. S. Jung and N. G. Park, Small **11**, 10 (2015).
[14]Y. J. Jiang, A. M. Soufiani, A. Gentle, F. Z. Huang, A. Ho-Baillie, and M. A. Green, Appl. Phys. Lett. **108**, 061905 (2016).
[15]W. W. Li, Z. G. Hu, J. D. Wu, J. Sun, M. Zhu, Z. Q. Zhu, and J. H. Chu, J. Phys. Chem. C **113**, 18347 (2009).
[16]Y. J. Jiang, M. A. Green, R. Sheng, and A. Ho-Baillie, Sol. Energy Mater. Sol. Cells **137**, 253 (2015).
[17]Q. Q. Lin, A. Armin, R. C. R. Nagiri, P. L. Burn, and P. Meredith, Nat. Photonics **9**, 106 (2015).
[18]M. Kato, T. Fujiseki, T. Miyadera, T. Sugita, S. Fujimoto, M. Tamakoshi, M. Chikamatsu, and H. Fujiwara, J. Appl. Phys. **121**, 115501 (2017).
[19]G. E. Jellison, Jr. and F. A. Modine, Appl. Phys. Lett. **69**, 371 (1996).
[20]W. W. Li, J. J. Zhu, X. F. Xu, K. Jiang, Z. G. Hu, M. Zhu, and J. H. Chu, J. Appl. Phys. **110**, 013504 (2011).
[21]D. O. Demchenko, N. Izyumskaya, M. Feneberg, V. Avrutin, Ü. Özgür, R. Goldhahn, and H. Morkoç, Phys. Rev. B **94**, 075206 (2016).
[22]M. Shirayama, H. Kadowaki, T. Miyadera, T. Sugita, M. Tamakoshi, M. Kato, T. Fujiseki, D. Murata, S. Hara, T. N. Murakami, S. Fujimoto, M. Chikamatsu, and H. Fujiwara, Phys. Rev. Appl. **5**, 014012 (2016).
[23]Y. X. Zhao and K. Zhu, Chem. Soc. Rev. **45**, 655 (2016).
[24]T. Umebayashi, K. Asai, T. Kondo, and A. Nakao, Phys. Rev. B **67**, 155405 (2003).
[25]W. Li, Z. M. Wang, F. Dechler, R. H. Freind, and A. K. Cheetham, Nat. Rev. Mater. **2**, 16099 (2017).
[26]A. M. A. Leguy, P. Azarhoosh, M. I. Alonso, M. Campoy-Quiles, O. J. Weber, J. Z. Yao, D. Bryant, M. T. Weller, J. Nelson, A. Walsh, M. Schilfgaarde, and P. R. F. Barnes, Nanoscale **8**, 6317 (2016).
[27]J. S. Park, S. K. Choi, Y. Yan, Y. Yang, J. M. Luther, S. H. Wei, P. Parilla, and K. Zhu, J. Phys. Chem. Lett. **6**, 4304 (2015).
[28]N. O. Yamamuro, T. Matsuo, and H. Suga, J. Phys. Chem. Solids **53**, 935 (1992).
[29]J. S. Manser, J. A. Christians, and P. V. Kamat, Chem. Rev. **116**, 12956 (2016).
[30]P. F. Ndione, Z. Li, and K. Zhu, J. Mater. Chem. C **4**, 775 (2016).